ADVANCED MATERIALS INTERFACES
Open Access
www.advmatinterfaces.de



# Bond Formation at Polycarbonate | X Interfaces (X = $Al_2O_3$, $TiO_2$, $TiAlO_2$) Studied by Theory and Experiments

*Lena Patterer,* Pavel Ondračka, Dimitri Bogdanovski, Stanislav Mráz, Peter J. Pöllmann, Soheil Karimi Aghda, Petr Vašina, and Jochen M. Schneider*

**Interfacial bond formation during sputter deposition of metal-oxide thin films onto polycarbonate (PC) is investigated by ab initio molecular dynamics simulations and X-ray photoelectron spectroscopy (XPS) analysis of PC|X interfaces (X = $Al_2O_3$, $TiO_2$, $TiAlO_2$). Generally, the predicted bond formation is consistent with the experimental data. For all three interfaces, the majority of bonds identified by XPS are (C—O)—metal bonds, whereas C—metal bonds are the minority. Compared to the PC|$Al_2O_3$ interface, the PC|$TiO_2$ and PC|$TiAlO_2$ interfaces exhibit a reduction in the measured interfacial bond density by 75 and ~65%, respectively. Multiplying the predicted bond strength with the corresponding experimentally determined interfacial bond density shows that $Al_2O_3$ exhibits the strongest interface with PC, while $TiO_2$ and $TiAlO_2$ exhibit ~70 and ~60% weaker interfaces, respectively. This can be understood by considering the complex interplay between the metal-oxide composition, the bond strength, and the population of bonds formed across the interface.**

## 1. Introduction

Poly(bisphenol A carbonate), generally referred to as polycarbonate (PC), is a thermoplastic polymer with many applications, for example, in the automotive industry, the medical sector, or in electrical components.[1] However, since PC is prone to stress corrosion cracking and sensitive to scratches, surface protection by thin films is often required.[2]

L. Patterer, D. Bogdanovski, S. Mráz, P. J. Pöllmann, S. Karimi Aghda, J. M. Schneider
Materials Chemistry
RWTH Aachen University
Kopernikusstr 10, 52074 Aachen, Germany
E-mail: patterer@mch.rwth-aachen.de

P. Ondračka, P. Vašina
Department of Physical Electronics
Faculty of Science
Masaryk University
Kotlářská 2, 61137 Brno, Czech Republic

The ORCID identification number(s) for the author(s) of this article can be found under https://doi.org/10.1002/admi.202400340



**DOI: 10.1002/admi.202400340**

Amorphous alumina ($Al_2O_3$) and titania ($TiO_2$) are suitable protective thin films due to their corrosion resistance[3,4] and significantly better mechanical properties ($E$ ~80–180 GPa[5,6]) compared to the rather soft PC ($E$ ~2 GPa[7]). Besides, both amorphous $Al_2O_3$ and $TiO_2$ have the advantage of being transparent, which widens their range of application as protective thin films for PC when transparency is required, such as safety goggles[1] or bulletproof windows.[8] Amorphous $Al_2O_3$ is already commonly used as a thin film in optical applications, such as optical lenses, antireflective coatings, and windows,[9] while amorphous $TiO_2$ is considered for applications in optoelectronic devices[10] or solar cells[11] and has been reported to be highly ductile if sufficiently dense and free of geometrical flaws.[12]

Protective thin films require good adhesion to the substrate to be effective, and the chemical bonding at the interface between PC substrates and thin films plays a crucial role in quantifying the adhesion properties.[13] Generally, PC consists of different functional groups that are potential interaction sites during the deposition of thin films: the (hydro-)carbon aromatic and aliphatic groups (C—C, C═C, C—H) as well as the carbonate group (O—(C═O)—O).[14]

A previous study demonstrated that the atomic layer deposition of amorphous $Al_2O_3$ and $TiO_2$ adhesion layers onto poly(methyl methacrylate) (PMMA) improved the adhesion of subsequently deposited Ti significantly when both layer thicknesses exceeded 33 nm.[15] Additionally, Gerenser[16] investigated the adhesion effect of plasma treatments prior to the deposition of Ag thin films onto polyethylene and presented the following adhesion trend of the used working gases: untreated < Ar < $O_2$ < $N_2$. This study showed that O and N play an essential role in interfacial bond formation by creating new reactive $CO_x$ and $CN_x$ groups.[16] However, Amor et al.[17] compared the X-ray photoelectron spectroscopy (XPS) spectra of an untreated and a $CO_2$-plasma-treated PMMA|$Al_2O_3$ interface (both with an alumina film thickness of ~1 nm) and showed that both samples exhibit a similar C 1s spectrum with respect to new interfacial $CO_x$ groups. These data suggest that a strongly adhering interface between the polymer and thin film does not necessarily require a prior plasma treatment in case of a metal-oxide deposition. This is also supported by an interfacial XPS study of $Al_2O_3$

**Table 1.** Chemical composition of thin films deposited onto Si for 30 min (EDX).

| | Al [at.%] | Ti [at.%] | O [at.%] |
|---|---|---|---|
| $Al_2O_3$ | 39 | – | 61 |
| $TiO_2$ | – | 37 | 63 |
| $TiAlO_2$ | 27 | 26 | 47 |

and $ZnO_2$ deposited onto PC,[18] demonstrating that upon reactive sputter deposition of a 1 nm thin film, new C—O and C═O groups are formed at both PC interfaces. However, more new C—O groups were introduced at the PC|$Al_2O_3$ interface, while more C═O groups were formed at the PC|$ZnO_2$ interface.[18] Therefore, the chemical composition of the metal oxide seems to be relevant for the interfacial group formation.

Due to the lack of systematic studies published on the interfacial bond formation of sputter-deposited alumina, titania, and a solid solution thereof onto PC, we present in the following an interfacial bond strength and population analysis of PC|X interfaces (X = $Al_2O_3$, $TiO_2$, $TiAlO_2$) by using ab initio simulations, electronic-structure-based bonding analyses and XPS experiments.

## 2. Results and Discussion

### 2.1. Thickness Calibration and Chemical Composition of Thin Films

Metal-oxide thin films deposited onto Si substrates for 30 min were analyzed with respect to their thickness and chemical composition. Measuring the film thickness from scanning electron microscopy (SEM) cross-sections, the nominal deposition rates of $1.0 \pm 0.1$, $16.8 \pm 0.1$, and $20.8 \pm 0.1$ nm $min^{-1}$ were determined for $Al_2O_3$, $TiO_2$, and $TiAlO_2$, respectively (Table S1, Supporting Information). To obtain thin films with a thickness of ~1 nm, deposition times of 60, 4, and 3 s were utilized for $Al_2O_3$, $TiO_2$, and $TiAlO_2$ onto PC, respectively. While it is possible that these films do not cover the PC substrates completely, it is evident that the applied methodology captures information pertaining to the nature of interfacial bonding. For the bond density calculations, a complete coverage is assumed. Hence, the here communicated bond density values formed between film and substrate provide a lower bound estimate, as a complete coverage would result in a larger interface area between film and substrate.

The chemical composition of the thin films was determined by energy dispersive X-ray spectroscopy (EDX) and is shown in **Table 1**. While the difference relative to the expected stoichiometry is only 4% for the standard-based $Al_2O_3$ measurement, the standardless measurements of $TiO_2$ and $TiAlO_2$ exhibit a greater deviation with ≤13%, which is, however, still within the systematic uncertainty of EDX.[19]

### 2.2. Simulated Sputter Deposition of Metal Oxides onto PC

Since a similar kinetic energy of sputtered species can be expected for DC and pulsed DC magnetron sputtering, ranging from a few eV for neutral atoms to tens of eV for ionized species (only ≤1% of all species),[20–22] the kinetic energy of all bombarding atoms in the ab initio simulations was set to 1 eV. As other deposition methods, like, e.g., atomic layer deposition (a few meV)[20] and high power pulsed magnetron sputtering (up to hundreds of eV)[22] can be categorized below and above this kinetic energy range, respectively, energy-dependent ab initio simulations would shed light on the interfacial bond formation with polymers under these conditions.

For the ab initio simulations, the interfaces of PC with the metal oxides are considered and compared to the pristine PC surface (**Figure 1**a). Figure 1b–d shows the plan view of the interfaces after the simulated sputter deposition of 6 formula units of $Al_2O_3$, 10 formula units of $TiO_2$, and 7.5 formula units of $TiAlO_2$ onto PC, respectively (30 atoms in total for each case). Comparing the interfaces with the pristine PC surface (Figure 1a), a significantly higher fraction of C—O groups is observed, indicating reactions of incident O atoms with the polymer. Additionally, C—metal bonds are visible, corresponding to the reaction of C atoms with both metal species, Al and Ti (Figure 1b–d). Due to the different stoichiometries of the thin films, the atomic oxygen-to-metal ratio is naturally the largest at the PC|$TiO_2$ interface (2/1), followed by PC|$Al_2O_3$ (3/2) and PC|$TiAlO_2$ (1/1).

### 2.3. Comparison of Calculated and Experimental C 1s Spectra

When analyzing the XPS survey scan of pristine PC, a surface concentration of ~84 at.% C and ~16 at.% O is measured, which is in good agreement with values from the literature (C/O = 83/17[26]). The calculated and measured C 1s spectra of pristine PC are depicted in **Figure 2**a,b, respectively, and both show signals of the C═C, C—C, and C—H (blue), the $C_{ring}$—O (orange), and the O—(C═O)—O (pink) groups. The binding energies (BEs) of the groups detected by XPS are in good agreement with BE values from literature,[14,26] including the two $\pi$–$\pi^*$ shake-up satellite signals detected at 291.5 and 292.5 eV associated with aromatic bonding[26] (Figure 2b). Also, the calculated BEs of the (hydro-)carbon and the $C_{ring}$—O groups at 284.6 and 286.1 eV, respectively, agree well with the XPS C 1s spectrum, whereas the BE shift (ΔBE) of the carbonate group (O—(C═O)—O) relative to the hydrocarbon group is underestimated by density functional theory (DFT) calculations ($\Delta BE_{DFT}$ = 4.7 eV versus $\Delta BE_{XPS}$ = 5.8 eV) (Figure 2a,b). This underestimation is likely due to method-related limitations such as the atomic-basis set or pseudopotential method used, as discussed in detail in our previous work on metal-nitride depositions onto PC.[24] Despite the BE differences between theory and experiment, the overall trend of the theoretical chemical shifts matches with the experimental spectrum (Figure 2).

As C is, besides H, the major constituent of PC, the changes in the C 1s spectrum play an essential role in probing the interfacial bonds forming with sputter-deposited thin-film atoms. By comparing the C 1s spectra of the interfaces to that of pristine PC, chemical state changes of C atoms upon deposition are investigated.

The theoretical and experimental C 1s spectra of the PC|$Al_2O_3$ interface are depicted in **Figure 3**a,b, respectively. The simulations predict interface formation via both interfacial (C—O)—Al

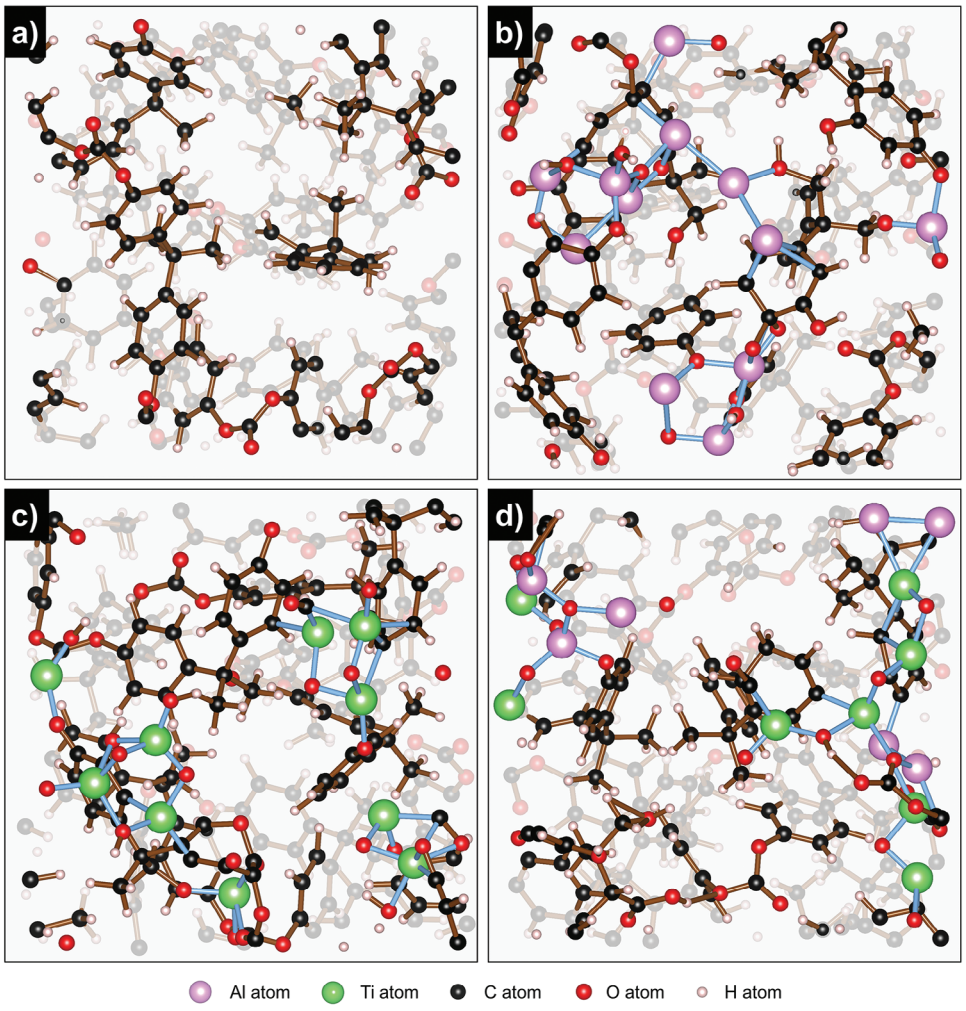


**Figure 1.** Plan view of a) pristine PC (Reproduced under terms of the CC-BY license.[23] 2023, Patterer et al.[24] published by Wiley-VCH), b) the PC|$Al_2O_3$, c) the PC|$TiO_2$, and d) the PC|$TiAlO_2$ interfaces visualized by VESTA.[25] The newly formed interfacial bonds are displayed in light blue.

(light blue, Figure 3a) and C—Al groups (yellow, Figure 3a). Experimentally (Figure 3b), the formation of (C—O)—Al and $CO_x$ groups is verified by three components detected between 285.8 and 289.5 eV (light blue, light-blue/brown-striped), while the C—Al component is detected at 282.2 eV (yellow).

To analyze the effect of pure O on the interfacial bond formation, an O-plasma treatment of PC substrates was carried out, and the resulting C 1s spectrum is shown in the supporting information (**Figure** S1). The C 1s spectrum of the O-plasma-treated PC looks very similar to the one coated by $Al_2O_3$, confirming that most interfacial bonds are formed by (C—O)—Al and $CO_x$ groups, connecting PC and the $Al_2O_3$ thin film. Generally, a higher BE of $CO_x$ groups means more O bonds attached to the C atom (e.g., BE (C═O) ~287.9 eV, BE (O—C═O) ~289.0 eV).[17] However, one difference between the C 1s spectra of the O-plasma treated PC and PC|$Al_2O_3$ is the light blue (C—O)—Al component at BE = 289.6 eV (Figure 3a), indicating the reaction of the pristine carbonate group (O—(C═O)—O) with Al atoms as previously observed.[27]

Considering the experimentally determined population of interfacial (C—O)—Al + $CO_x$ groups (Figure 3b), indicated by the area fraction of the light blue and light-blue/brown components, it is ~80 times larger than the area fraction of the C—Al groups (yellow component). This is in contrast to the calculated C 1s spectrum, which predicts nearly the same population of C—Al and (C—O)—Al groups (Figure 3a) and may indicate that the O concentration at the experimental interface is significantly higher compared to the stoichiometric $Al_2O_3$ ratio assumed for the simulations.

To estimate the interfacial oxygen-to-metal ratio of the thin film, the carbon concentration was quantified using the survey spectrum of the interface samples and assuming an atomic oxygen-to-carbon ratio of 84/16 for PC (value measured for pristine PC) as well as an adventitious carbon concentration of zero. The oxygen concentration ascribed to the thin film was determined by subtracting the oxygen content ascribed to the signal of pristine PC from the overall oxygen concentration measured for the interface sample. Analyzing the survey scan after a 4 s deposition of $Al_2O_3$ onto PC (thickness ~0.1 nm) indicates an atomic concentration of deposited O at the interface that is ~4.5 times higher than that of Al (the stoichiometric ratio assumed for the simulation is O/Al = 1.5). A similar experimental observation

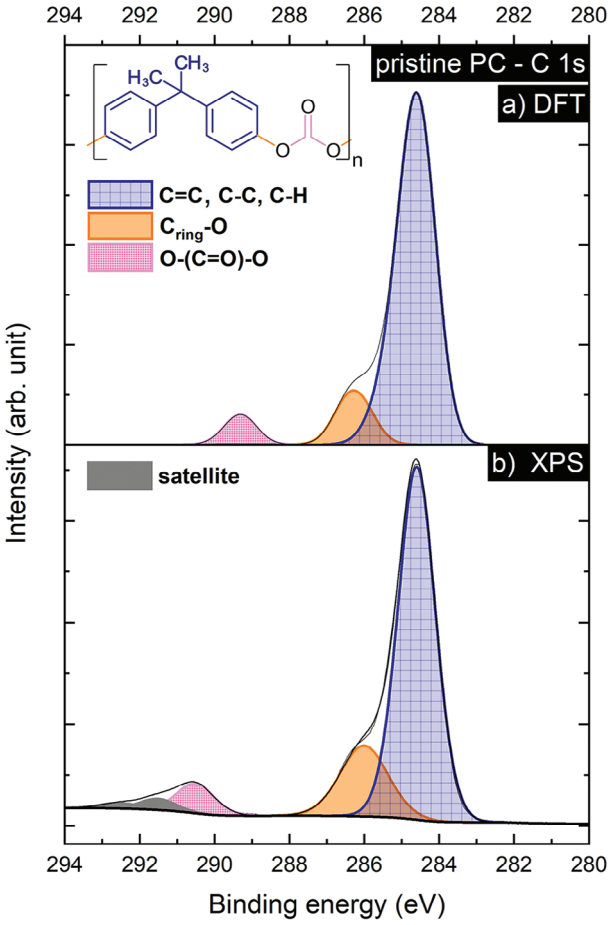


**Figure 2.** C 1s spectra of pristine PC a) calculated by DFT based on the PC bulk model depicted in Figure 1a, and b) measured by XPS (Reproduced under terms of the CC-BY license.[23] 2023, Patterer et al.[24] published by Wiley-VCH).

was made for the metal-nitride depositions, showing a significantly higher fraction of C—N than C—metal groups.[24,28] These diverging chemical compositions at the interface also agree well with reports from literature, observing an interfacial layer of ~5 nm thickness for metallic Al and Ti thin films deposited on polymers that exhibit a different chemical composition compared to the thin film growing after reaching a thickness of 5 nm.[29,30]

Hence, while these simulations predict that interfacial groups are formed very well, the population of these groups might differ compared to the experiment due to diverging O/metal ratios at the simulated versus experimental interfaces.

Considering the PC|$TiO_2$ interface, the calculated and experimentally detected C 1s spectra are depicted in **Figure** 4a,b, respectively. The PC|$TiO_2$ simulation predicts an interface formation via C—Ti bonds (green component) and (C—O)—Ti bonds (red component), while both components exhibit a similar BE of ~282.4.–283.9 and ~284.2 eV, respectively (Figure 4a).

The experimental C 1s spectrum of the PC|$TiO_2$ interface also shows evidence of the C—Ti component at BE = 282.2 eV (Figure 4b); however, the numerous experimentally detected (C—O)—Ti groups with distinct signals (red, brown/red-striped, orange/red-striped) exhibit higher BEs (285.8–289.1 eV) compared to the predicted groups (Figure 4a), indicating higher oxygen concentration within the groups.[17]

Despite the similarities of the experimental C 1s spectra of PC|$Al_2O_3$ and PC|$TiO_2$, it is evident that significantly more (C—O)—metal + $CO_x$ groups are formed upon $Al_2O_3$ deposition compared to the $TiO_2$ case. Analyzing the survey scan after the deposition of $TiO_2$ onto PC for 0.5 s (thickness ~0.1 nm), an O/Ti ratio of 2.5 is obtained, which is close to the stoichiometric ratio of 2 assumed for the simulations. This indicates that the initial O/metal ratio at the PC|$TiO_2$ interface (2.5) is lower compared to the one at the PC|$Al_2O_3$ interface (4.5).

The experimental and simulated C 1s spectra of the PC|$TiAlO_2$ interface show similar results compared to the PC|$Al_2O_3$ and PC|$TiO_2$ interfaces, as the presence of (C—O)—metal and C—metals bonds is observed. Both PC|$TiAlO_2$ spectra are depicted in the supporting information (**Figure** S2).

To obtain more insights into the mechanisms of the interfacial bond formation with regard to similarities and differences, the O 1s spectra of interfaces with thinner film thickness (<0.2 nm) are analyzed in the next step of this study.

### 2.4. Comparison of Calculated and Experimental O 1s Spectra

While the analysis of the C 1s components was conducted to quantify the interfacial bonding type after the deposition of 1 nm film thickness, the O 1s spectra were investigated to verify the oxygen-based interfacial components as well as examine the thin film growth relative to the interface formation. Thus, a thinner film thickness of <0.2 nm was considered for the analysis of the O 1s spectra.

A pristine PC monomer exhibits two O 1s contributions (**Figure** 5a): one double-bonded O atom (C=O) at BE = 532.3 eV and two single-bonded O atoms ($C_{ring}$—O—C) at BE = 533.9 eV.[31] When the sputter deposition of $Al_2O_3$ onto PC is simulated, the calculated O 1s spectrum (Figure 5b-i) exhibits, besides the pristine O=C (pink) and $C_{ring}$—O—C groups (orange), additional contributions of interfacial C—O—Al groups (light blue), thin-film related O—Al groups within the growing thin film (salmon), and various gaseous $CH_xO_y$ molecules (grey). The interfacial C—O—Al groups exhibit BEs in the range of ~530.3–533.8 eV, implying reactions with mostly single-bonded O (light blue contributions at >532.2 eV) but also some reactions with double-bonded O (light blue contributions at <532.2 eV). Both the C—O—C and the O=C groups are shifted toward lower BE upon interacting with Al atoms due to a lower oxidation state. As the electronegative O atoms attract the electrons of the Al atoms, the electron density of the O atoms is increased, and thus, the electron attraction by the nucleus is reduced. In this way, the BE of the O atoms is decreased, as less energy is required to remove core electrons.[32,33]

The experimentally detected O 1s spectrum of PC|$Al_2O_3$ (Figure 5b-ii) constitutes a symmetric peak shape. Nevertheless, two distinct components are identified, with the component at a higher BE of ~533.2 eV attributed to C—O—C and C—O—Al contributions (orange/blue striped). In comparison, the component at lower BE of ~533.2 eV is assigned to O=C and O—Al contributions (pink/salmon striped, Figure 5b-ii).

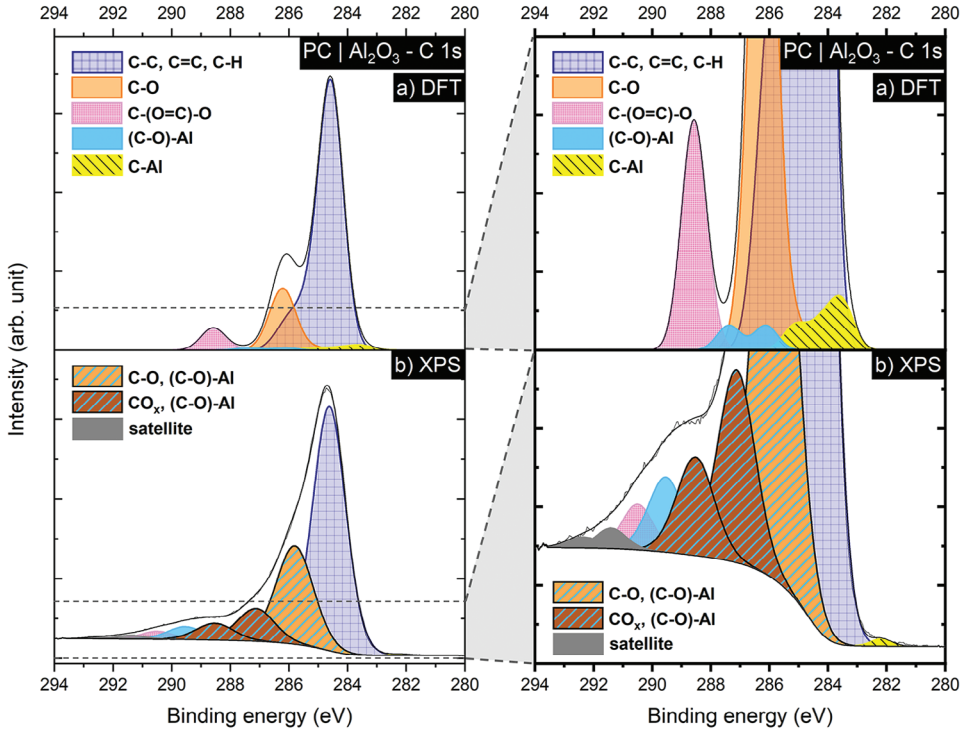


**Figure 3.** The C 1s spectra of the PC|$Al_2O_3$ interface as a) calculated by DFT and b) measured by XPS. On the left, the complete spectra are shown, while on the right, a magnification of the low-intensity C 1s components is depicted. The different groups are indicated by the color code provided in the legend.

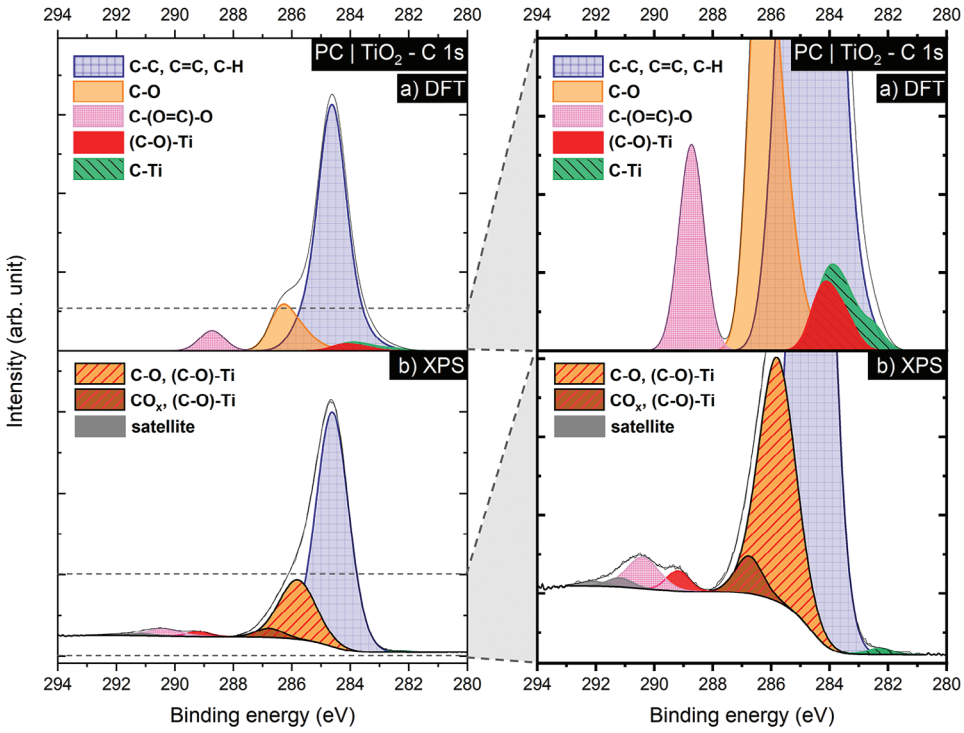


**Figure 4.** The C 1s spectra of the PC|$TiO_2$ interface as a) calculated by DFT and b) measured by XPS. On the left, the complete spectra are shown, while on the right, a magnification of the low-intensity C 1s components is depicted. The different groups are indicated by the color code provided in the legend.

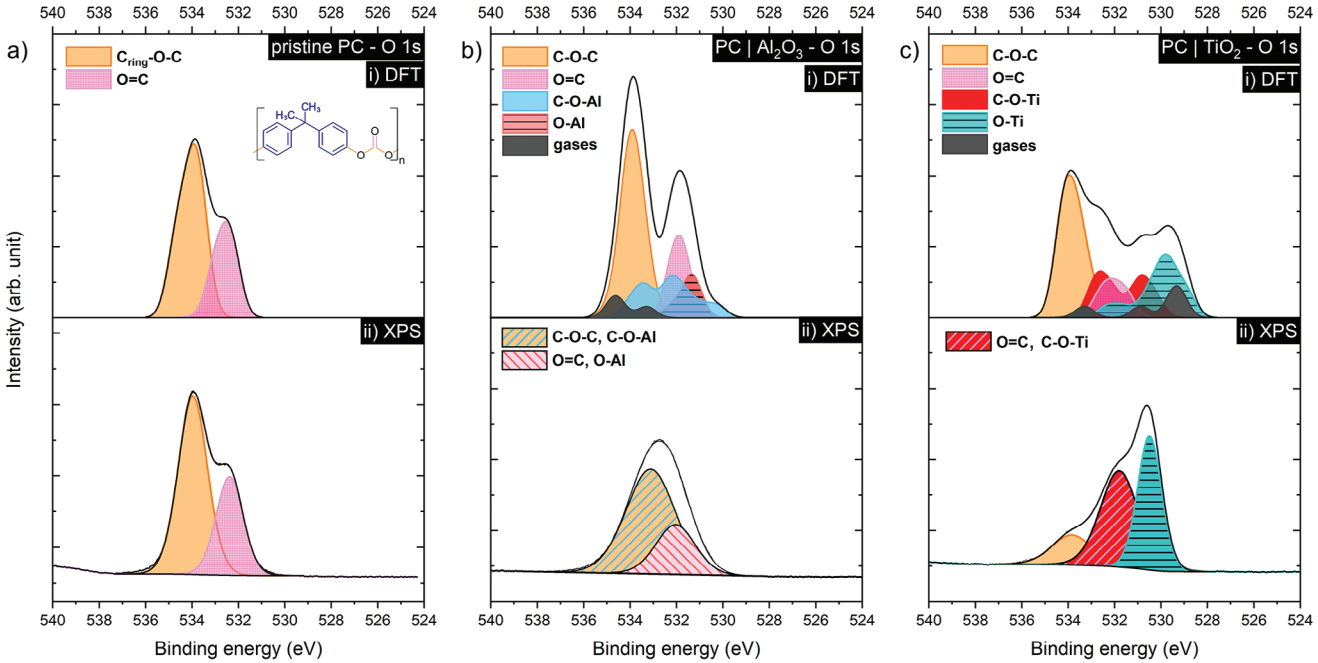


**Figure 5.** The O 1s spectra of a) pristine PC, b) the PC|$Al_2O_3$ interface, and c) the PC|$TiO_2$ interface determined i) by DFT calculations and ii) by XPS measurements. The different groups are indicated by the color code provided in the legend.

When $TiO_2$ is deposited onto PC, the simulation predicts two main C—O—Ti contributions at BE ~532.5 and ~530.8 eV (both red), indicating the reaction with the single- and double-bonded O groups, respectively (Figure 5c-i). When the chemical environment of O is defined exclusively by Ti atoms, a component at BE ~529.8 eV is determined (turquoise, Figure 5c-i). Additionally, the formation of various gaseous $CH_xO_y$ compounds is observed after the simulation (grey components, Figure 5c-i).

Overall, the predicted O 1s spectrum for PC|$TiO_2$ is wider (~4 eV between C—O—C and O—Ti, Figure 5c-i) compared to the O 1s spectrum of PC|$Al_2O_3$ (~2.5 eV between C—O—C and O—Al, Figure 5b-i). This can be explained by the larger electronegativity differences between Ti (1.54) and C (2.55) compared to Al (1.61) and C.[34] A similar trend was previously observed for the N 1s spectra of AlN and TiN.[24] The wider O 1s spectrum of the experimental PC|$TiO_2$ allows for a better distinction of the individual O 1s contributions (Figure 5c-ii).

The component at the highest BE ~533.9 eV of the experimental O 1s spectrum is attributed to the pristine single-bonded O groups of PC (orange), whereas the largest component at BE ~530.4 eV is attributed to the growing $TiO_2$ thin film (turquoise, Figure 5c-ii). The component at BE ~531.8 eV (red/pink striped) is assigned mainly to interfacial C—O—Ti groups, as well as a small contribution of C=O groups, although the latter should constitute only ~50% of the area detected for the C—O—C component (compare Figure 5a).

When comparing the experimental O 1s spectra of both interfaces, it is evident that the O—Ti component (turquoise), corresponding to the growing thin film, constitutes a higher area fraction compared to the corresponding thin-film component of $Al_2O_3$ (pink/salmon striped). Since both XPS O 1s spectra reflect the interface state after the deposition of thin films with a similar thickness (<0.2 nm for both $Al_2O_3$ and $TiO_2$), $TiO_2$ seems to form a thin film covering the interfacial region earlier compared to $Al_2O_3$. Accordingly, the simulations predict a higher O—Ti population (turquoise component) relative to the O—Al population (purple component) after the deposition of 30 atoms (Figure 5b-i,c-i with same y-axis dimensions), thus indicating a higher tendency of O to form O—Ti groups compared to O—Al groups.

The XPS O 1s spectrum of the PC|$TiAlO_2$ interface constitutes an intermediate state of the $Al_2O_3$ and $TiO_2$ systems, as it consists mainly of C—O—(Ti,Al) bonds and a smaller fraction of O—Ti and C—O—C bonds (**Figure** S3, supporting information).

### 2.5. Interfacial Bond Density

For the experimental evaluation of the interfacial bond density, the relative area of the interfacial C 1s components formed upon the deposition of a 1 nm-thick film onto PC was determined according to our previously proposed method:[24]

$$C\ 1s\ interfacial\ component\ fraction\ (\%) = \frac{Area\ of\ interfacial\ C\ 1s\ component}{Area\ of\ whole\ C\ 1s\ signal} \times 100 \quad (1)$$

**Figure 6** compares the *C 1s interfacial component fraction* of the three PC | X interfaces (X = $Al_2O_3$, $TiO_2$, $TiAlO_2$) and subcategorizes the different interfacial bond types. Due to the formation of many (C—O)—Al bonds, the PC | $Al_2O_3$ interface has the highest *C 1s interfacial component fraction* – or, stated in a simpler term – the highest interfacial bond density. In comparison,

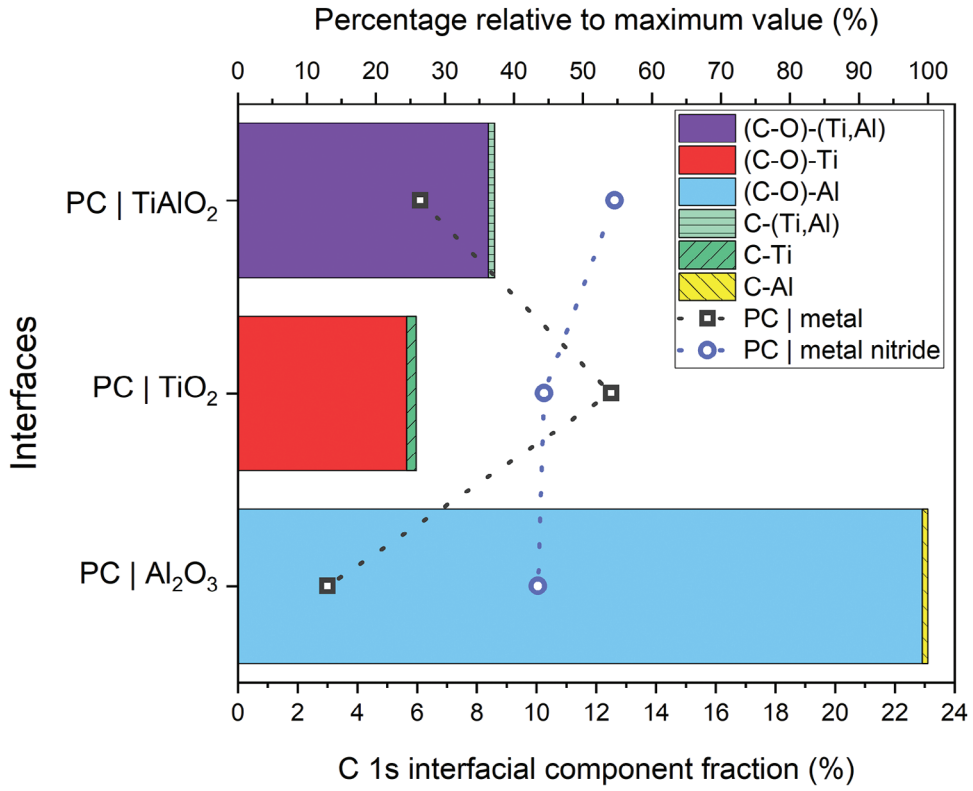


**Figure 6.** The *C 1s interfacial component fraction* of the individual interfacial groups is depicted for the PC | X3 interfaces (X3 = $Al_2O_3$, $TiO_2$, $TiAlO_2$), categorized by the color code provided in the legend. For comparison, the cumulative *C 1s interfacial component fractions* of the PC | X1 (X1 = Al, Ti, TiAl)[27] and PC | X2 (X2 = AlN, TiN, (Ti,Al)N)[24] interfaces are shown as grey squares and blue circles, respectively. Lines between data points are depicted as a guide for the eye.

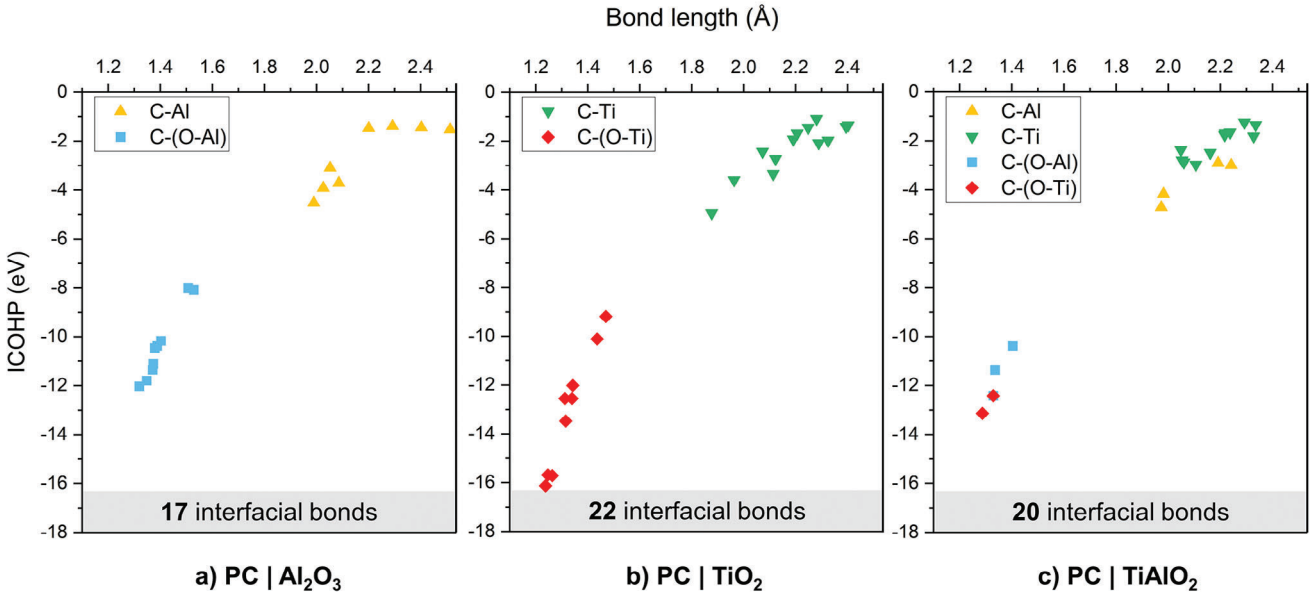


**Figure 7.** ICOHP values (bond strength) of individual interfacial bonds for the simulated a) PC | $Al_2O_3$, b) PC | $TiO_2$, and c) PC | $TiAlO_2$ interfaces, as well as their cumulative number of interfacial bonds at the final state of the sputter deposition simulation.

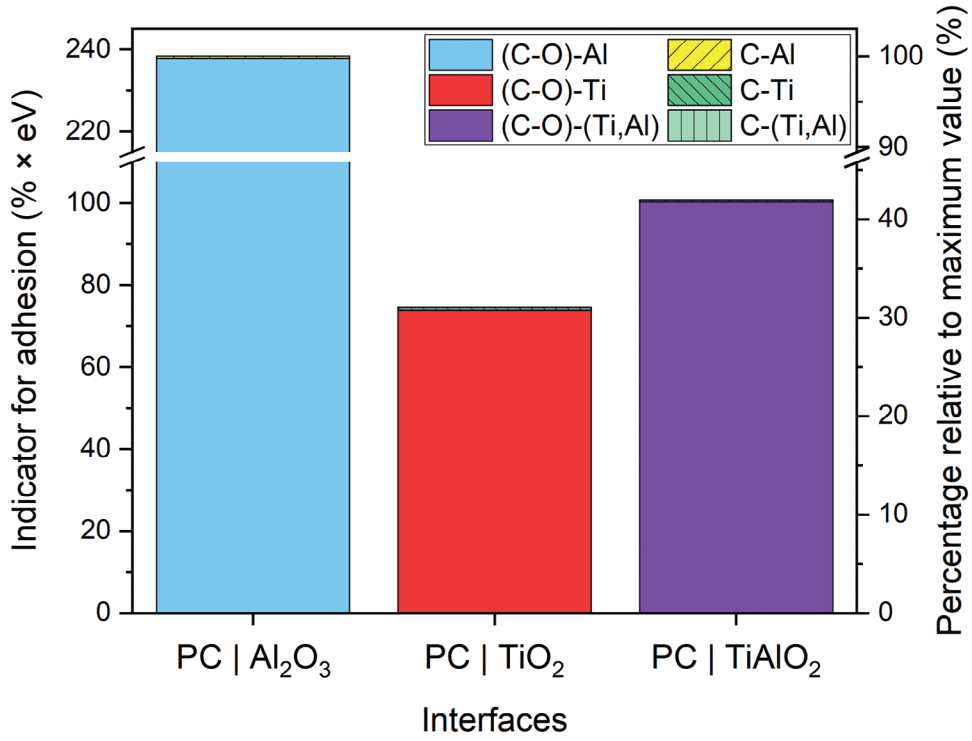


**Figure 8.** The *indicator for adhesion* of the PC | X interfaces (X = $Al_2O_3$, $TiO_2$, $TiAlO_2$) combines the measured relative interfacial bond density and the absolute ICOHP values of the respective bond type. The values for the different groups are indicated by the color code provided in the legend. Axis breaks between 110–215% × eV (left axis) and 45–90% (right axis) are utilized for better visibility.

PC | $TiO_2$ and PC | $TiAlO_2$ exhibit ~75 and ~65% less interfacial bonds, respectively (Figure 6). Also, compared to the corresponding metallic[27] and the metal-nitride systems,[24] substantially more interfacial bonds are formed at the PC | $Al_2O_3$ interface (Figure 6).

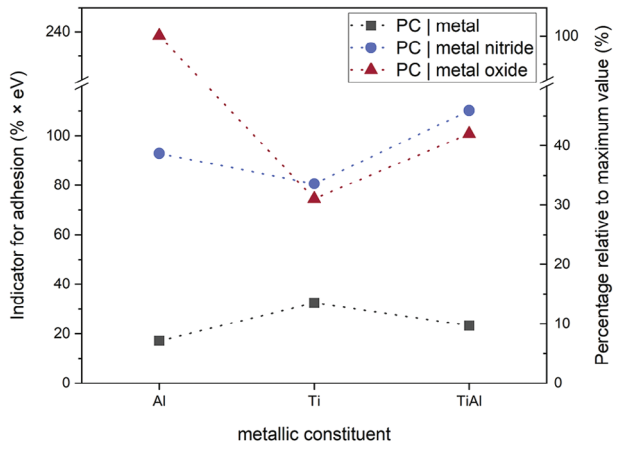


**Figure 9.** The cumulative indicator for adhesion of the PC | X1 (X1 = Al, Ti, TiAl),[27] the PC | X2 (X2 = AlN, TiN, (Ti,Al)N),[24] and the PC | X3 (X3 = $Al_2O_3$, $TiO_2$, $TiAlO_2$) interfaces is depicted as grey squares, blue circles, and red triangles, respectively. The indicator for adhesion is based on the calculated ICOHP values multiplied by the interfacial bond density determined experimentally after the deposition of ~1 nm film thickness. Axis breaks between 120–220% × eV (left axis) and 50–92% (right axis) are used for better visibility, while lines connecting the symbols are depicted as a guide for the eye.

### 2.6. Interfacial Bond Strength Analysis (ICOHP)

To evaluate the interfacial bond strength, integrated crystal orbital Hamilton population (ICOHP) calculations were performed for the simulated PC | $Al_2O_3$, PC | $TiO_2$, and PC | $TiAlO_2$ interfaces. The calculated ICOHP values for the corresponding interfacial bonds are depicted as a function of bond length and interacting atoms in **Figure 7**. Generally, a more negative (or larger absolute) ICOHP value implies a stronger bond. As shown in Figure 7, the C-metal bonds exhibit a weaker bond strength (ICOHP between −1.1 and −5.0 eV) compared to the C—(O—metal) bonds (between −8.0 and −16.1 eV). The C—(O—metal) bonds correspond to the ICOHP value between a C and an O atom, while the O atom is, in this case, also bonded to a metal atom, thus forming an interfacial bond between the thin film and PC. These strong ICOHP values for the C—(O—Al) bonds agree well with reports from literature, observing stable Al | polymer interfaces due to the formation of stable Al—O—C complexes, enduring even elevated temperatures.[35] In contrast, literature suggests less stable interface components for Ti-based thin films deposited onto polymers that degrade upon heat treatment.[30]

Additionally, the simulations predict a higher interfacial bond density for the PC | $TiO_2$ interface (22 interfacial bonds/30 deposited atoms) compared to the PC | $Al_2O_3$ interface (17 interfacial bonds/30 deposited atoms) due to the higher number

**Table 2.** Ar and $O_2$ partial pressures during different metal-oxide depositions.

| Partial pressure | $Al_2O_3$ | $TiO_2$ | $TiAlO_2$ |
|---|---|---|---|
| $p_{Ar}$ [Pa] | 0.53 | 0.53 | 0.68 |
| $p_{O2}$ [Pa] | 0.08 | 0.03 | 0.03 |

of C—Ti bonds (number of green data points) compared to the fewer C—Al bonds (number of yellow data points) (Figure 7). The PC | $TiAlO_2$ interface exhibits a number in between (20 interfacial bonds/30 deposited atoms). This deviating trend from the experimentally measured interfacial bond density (Figure 6) can be explained by a different initial O/metal ratio at the interface during the experimental sputter deposition, as discussed before.

### 2.7. Indicator for Adhesion

To compare the interfacial strength, the *indicator for adhesion* was defined previously,[27] corresponding to the average absolute ICOHP value for each bond type (**Figure 7**) multiplied by the experimentally determined *C 1s interfacial component fraction* (Figure 6). More details on the calculations of the *indicator for adhesion* can be found in the supporting information (Table S2).

By comparing the *indicator for adhesion* for the PC | X interfaces (X = $Al_2O_3$, $TiO_2$, $TiAlO_2$) (**Figure 8**), the strongest interfacial bond formation is determined for $Al_2O_3$, due to the numerous strong (C—O)—Al bonds (see Figure 6). The second strongest interface is formed for PC | $TiAlO_2$, while PC | $TiO_2$ shows the weakest interface formation (Figure 8). For all three interfaces, the main contributions to the *indicator for adhesion* are defined by interfacial (C—O)—metal bonds, whereas C—metal bonds play a negligible role due to their low detected density (see Figure 6), as well as their weaker bond strength (see **Figure 7**).

When comparing the overall values of the *indicator for adhesion* for the PC interface with sputter-deposited metals (Al, Ti, TiAl),[27] metal nitrides (AlN, TiN, (Ti,Al)N),[24] and metal oxides ($Al_2O_3$, $TiO_2$, $TiAlO_2$) some additional trends can be observed (**Figure 9**). Based on Figure 9, the metallic systems form weaker interfaces with PC compared to the metal-nitride and metal-oxide systems. Since PC | Ti exhibits a similar or higher interfacial bond density compared to the metal-nitride and metal-oxide systems (Figure 6), the weaker interfacial bond strength of the metal-based bonds is the reason for the lower *indicator for adhesion*. In contrast, the rather strong interfacial N-based and O-based bonds lead to stronger interfaces for the metal-nitride and metal-oxide systems. This observation is also in good agreement with literature reporting better adhesion for metals (Ag) deposited onto N- or O-plasma-treated polymer surfaces compared to the depositions onto untreated or Ar-treated surfaces.[16]

Additionally, it is observed in Figure 9 that TiN and $TiO_2$, as well as (Ti,Al)N and $TiAlO_2$ show similar values for the *indicator for adhesion*, while the nitride systems in both cases exhibit a slightly higher value compared to the oxide systems. Also, this trend is in good agreement with previous reports in literature.[16,36] The simulations showed that both N and O form strong bonds at the PC interface with similar ICOHP values. However, the interfacial XPS analysis of the C 1s spectra conducted for TiN and $TiO_2$, as well as for (Ti,Al)N and $TiAlO_2$, reveal a higher concentration of N-based interfacial bonds than the O-based interfacial bonds. In agreement with this, the simulations indicate that a significantly higher interfacial bond density is formed after the deposition of TiN (34 bonds/30 deposited atoms)[24] compared to $TiO_2$ (22 bonds/30 deposited atoms). One explanation might be that O has – compared to N – a higher tendency to form bonds with Ti. When comparing both configurations after the simulations, only 1 out of 18 formed N—Ti bonds is not part of a bridging C—N—Ti group. Contrarily, 18 out of 29 formed O—Ti bonds are not part of a bridging C—O—Ti connection. Hence, O has, compared to N, a higher tendency to form bonds with Ti exclusively, and thus, contributes less to the interfacial bond formation between thin film and polymer.

When comparing the trends of the *indicator for adhesion* among the metals, metal nitrides, and metal oxides, it is evident that Ti forms the strongest interface among the metals. However, for TiN and $TiO_2$, the weakest interfacial bond formation is observed among the metal nitrides and metal oxides, respectively. As already discussed in our previous study,[24] it seems that the high reactivity of both Ti and N leads to fewer strong C—N bonds, while numerous weak Ti-based interfacial bonds are formed instead. The same trend seems to be valid for the $TiO_2$ systems and is enhanced by the high tendency to form O—Ti rather than bridging C—O—Ti bonds.

The overall highest *indicator for adhesion* is determined for PC | $Al_2O_3$, which is more than twice as high compared to the second strongest interface (PC | (Ti,Al)N). The higher *indicator for adhesion* for AlN compared to TiN was explained by the low reactivity of Al to form bonds with the hydrocarbon groups of PC, thus leading to many strong C—N bonds at the interface.[24] Similarly, the high concentration of bridging interfacial C—O—Al is the main reason for the high *indicator for adhesion* of the PC | $Al_2O_3$ interface.

## 3. Conclusion

This study compared the interfacial bond formation of sputter-deposited $Al_2O_3$, $TiO_2$, and $TiAlO_2$ thin films onto PC substrates by correlative ab initio simulations and XPS measurements. While the predicted formation of interfacial C—metal and (C—O)—metal groups by simulations was confirmed by XPS, their populations deviated from predictions due to an experimentally higher initial O/metal ratio. While for the PC | $Al_2O_3$ interface, a high density of (C—O)—Al groups is detected by XPS, the interfacial bond density detected at the PC | $TiAlO_2$ and PC | $TiO_2$ interfaces is ~65 and ~75% lower, respectively. Due to the significantly higher concentration of interfacial bonds, the *indicator for adhesion* – a measure combining the calculated bond strength with the XPS-measured interfacial bond density – is also highest for the PC | $Al_2O_3$ interface, followed by a ~60% weaker PC | $TiAlO_2$ interface, as well as a ~70% weaker PC | $TiO_2$ interface. Comparing the *indicator of adhesion* for metal oxides ($Al_2O_3$, $TiO_2$, $TiAlO_2$), metals (Al, Ti, TiAl), and metal nitrides (AlN, TiN, (Ti,Al)N), additional mechanisms and trends are identified to form strong interfaces with PC:

- The strongest PC | metal interface is obtained for Ti, due to the largest interfacial bond density. Even though Al forms stronger interfacial bonds than Ti, its lower interfacial bond density leads to the weakest interface.
- Among the metal-nitride systems, TiN exhibits approximately the same interfacial bond density as AlN. Still, fewer strong C—N bonds are formed at the PC | TiN interface, leading to an overall weaker interface compared to PC | AlN.
- A high initial O/metal or N/metal ratio is preferential for a strong interface formation of metal oxides or metal nitrides deposited onto PC due to the high interfacial bond density of strong C—N and C—O groups.

## 4. Experimental Section

*Experimental Methods*: PC substrates were prepared by using 5 wt.% PC pellets (additive-free, product # 4 315 139, Sigma–Aldrich) dissolved in tetrahydrofuran (anhydrous, 99.9% purity, inhibitor-free, Sigma–Aldrich). The solution was spin-coated onto 10 × 10 $mm^2$ fused-silica substrates (Siegert Wafer GmbH) by applying a velocity of 2000 rpm. Immediately after preparation, the substrates were mounted into the evacuated deposition chamber to reduce the influence of surface contamination. Additionally, thin films deposited onto conductive 10 × 10 $mm^2$ Si (100) substrates (Crystal GmbH) were analyzed regarding the film thickness, and thus, deposition rate, as well as the chemical composition.

The utilized Ti, Al, and composite $Ti_{50}Al_{50}$ deposition targets (purity ≥99.995% in each case) had a diameter of 50 mm and were mounted with a target-to-substrate distance of 100 mm, while the angle between target normal and substrate normal was 45°. The base pressure before the deposition was always ≤$7 \times 10^{-5}$ Pa, and the Ar and $O_2$ partial pressures (both gases ≥99.99% purity) were set during the respective sputter deposition according to **Table 2** in order to obtain the aimed stoichiometric compositions. To ensure a homogenous deposition, the substrate was rotated at 28 rpm during deposition. No intentional substrate heating was applied.

While pulsed direct current magnetron sputtering (PDCMS) was used for the $Al_2O_3$ and $TiAlO_2$ depositions (frequency = 250 kHz, $t_{OFF}$ = 1616 ns) to avoid arcing at the target, the $TiO_2$ deposition was run in DC mode. The time-averaged power density applied to each target was 10.2 W $cm^{-2}$. Before each deposition, target sputter cleaning was performed behind a closed shutter for ≥2 min.

After deposition, the samples were transferred from the deposition chamber to the XPS load-lock chamber with an atmosphere exposure time of <5 min. Although the presence of adventitious carbon on the surface during the atmosphere exposure time was expected, its influence on the C 1s signal was assumed to be marginal and similar for all samples as the exposure time was minimized. XPS measurements were carried out using an AXIS Supra (Kratos Analytical Ltd.) equipped with a monochromatic Al-K$\alpha$ source and a hemispherical detector. The base pressure during acquisition was always <$2 \times 10^{-6}$ Pa. The size of the XPS measurement spot was 700 µm × 300 µm. High-resolution spectra (C 1s, O 1s) were acquired using a pass energy of 20 eV (step size 0.05 eV, dwell time 100 ms, 20 sweeps), while for survey scans, a pass energy of 160 eV was employed (step size 0.25 eV, dwell time 100 ms, 5 sweeps). To avoid charging effects, charge neutralization was applied using a low-energy, electron-only source, and the BE scale was calibrated with respect to the hydrocarbon signal of PC at 284.6 eV.[26] The analysis of the XPS data was conducted using the CasaXPS software package 2.3.15 (Casa Software Ltd.), subtracting a Shirley background[37] and applying the manufacturer's sensitivity factors[38] for chemical quantification. The components of the C 1s and O 1s spectra were fitted with a Gaussian-Lorentzian (70%–30%) line shape, and the full width at half maximum (FWHM) of the C 1s components was constrained to ≤1.5 eV.[26]

The analysis of the C 1s spectra aims to quantify the interfacial components. In order to compare the interfacial bond density among the different thin film systems, interface samples after the deposition of ~1 nm film thickness onto PC were considered. The analysis of the O 1s spectra, however, aims to elucidate the progress of the thin film growth relative to the interface formation, and therefore, interfaces with a lower film thickness were considered (<0.2 nm). These thin films were obtained by using fast-acting shutters in front of the targets with an actuation time of 200 ms.

Thickness measurements were performed using an FEI Helios Nanolab 660 equipped with a field emission microscope to analyze the cross-sections of thin films deposited onto Si for 30 min. For the SEM image acquisition, an acceleration voltage and current of 10 kV and 50 pA were applied, respectively.

To determine the chemical composition of the thin films deposited onto Si for 30 min, EDX was conducted by using a TM4000Plus Tabletop scanning electron microscope (Hitachi Ltd.) equipped with a Quantax75 detector and applying a 10 kV acceleration voltage. For the quantification of the $Al_2O_3$ thin film, a $Al_2O_3$ (0001) substrate (Crystal GmbH) was used as a standard, whereas the $TiO_2$ and $TiAlO_2$ thin films were quantified standardless.

*Computational Methods*: Simulations of $Al_2O_3$, $TiO_2$, and $TiAlO_2$ sputter depositions onto PC were conducted by DFT-based ab initio molecular dynamics (AIMD) using the OpenMX package.[39–42] The PBE exchange-correlation potential[43] was utilized along with the DFT-D3 dispersion correction[44] to accurately model the van-der-Waals interactions. Methodological details on creating the PC bulk model consisting of 396 atoms are given in Ref. [24]. For the sputter-deposition simulation, the PC surface was bombarded by 30 atoms, each with a kinetic energy of 1 eV (kinetic energy of DC-sputtered atoms was typically in the range of a few eV[21]). An atomic sequence of O-Al-O-O-Al in terms of incident atoms was used for the $Al_2O_3$ deposition simulation, while a sequence of Ti-O-O and O-Ti-O-Al was applied for $TiO_2$ and $TiAlO_2$, respectively. The time interval between the incident atoms was 500 fs, and the temperature during the simulation was kept constant at 300 K (close to room temperature). After the deposition of 30 atoms, the final configuration was relaxed and subsequently utilized to calculate the C 1s and O 1s core electron BEs by using the core-hole approach.[45] More details on the calculations can be found elsewhere,[24] and all calculation data were available in the NOMAD archive.[46,47]

Bonding analysis was carried out by crystal orbital Hamilton population (COHP)[48] calculations using the LOBSTER package (version 4.0.0)[49–51] for projection of atom-resolved, local orbitals from delocalized plane-wave basis sets. The required wavefunctions post-processed with LOBSTER were obtained from static simulation runs using the Vienna ab initio simulation package (VASP, version 5.4.4).[52–54] To prepare the required structural model, the final structure of the respective AIMD simulation (PC + deposited atoms) was excised with a distance of 13 Å from the basal plane to reduce the system size and to ensure acceptable computational time and costs. Using this simplified structure, the static VASP simulation run provided the wavefunction from which COHP calculations via LOBSTER obtained the atom-resolved orbital information, and thus, the bonding characteristics. The integrated COHP values (ICOHP) per bond were extracted and interpreted as an indirect but strongly correlated indicator of bond strength.[55,56] More computational details on the ICOHP calculation methodology can be found in Ref. [24].

## Supporting Information

Supporting Information is available from the Wiley Online Library or from the author.

## Acknowledgements

This research was funded by the German Research Foundation (DFG, SFB-TR 87/3) "Pulsed high power plasmas for the synthesis of nanostructured functional layers" and project LM2023039 funded by the Ministry of Education, Youth and Sports of the Czech Republic. The authors gratefully acknowledge the computing time and support provided by the IT Center

of RWTH Aachen University and granted by the Jülich-Aachen Research Alliance (JARA) within the framework of the JARA0151 and JARA0221 projects.

## Conflict of Interest

The authors declare no conflict of interest.

## Author Contributions

L.P. performed conceptualization, methodology, formal analysis, investigation, writing – original draft, visualization. P.O. performed methodology, formal analysis, investigation, writing – original draft. D.B. performed methodology, formal analysis, investigation, writing – original draft. S.M. performed methodology, investigation, writing – review & editing. P.J.P. performed formal analysis, investigation, writing – review & editing, S.K.A. performed formal analysis, investigation, writing – review & editing. P.V. performed supervision, funding acquisition, writing – review & editing. J.M.S. performed conceptualization, methodology, writing – original draft, supervision, project administration, funding acquisition.

## Data Availability Statement

The data that support the findings of this study are available from the corresponding author upon reasonable request.

## Keywords

*ab initio* molecular dynamics, density functional theory, metal oxides, polycarbonate, sputter deposition, X-ray photoelectron spectroscopy

Received: April 20, 2024
Revised: June 18, 2024
Published online:

[1] D. Kyriacos, *Brydson's Plastics Materials*, Elsevier, Amsterdam, Netherlands **2017**, p. 457.
[2] A. Kausar, *J. Plast. Film Sheeting* **2018**, *34*, 60.
[3] C. X. Shan, X. Hou, K.-L. Choy, *Surf. Coat. Technol.* **2008**, *202*, 2399.
[4] P. Boryło, K. Lukaszkowicz, M. Szindler, J. Kubacki, K. Balin, M. Basiaga, J. Szewczenko, *Vacuum* **2016**, *131*, 319.
[5] J. Lyytinen, X. Liu, O. M. Ylivaara, S. Sintonen, A. Iyer, S. Ali, J. Julin, H. Lipsanen, T. Sajavaara, R. L. Puurunen, J. Koskinen, *Wear* **2015**, *342–343*, 270.
[6] A. van der Rest, H. Idrissi, F. Henry, A. Favache, D. Schryvers, J. Proost, J.-P. Raskin, Q. van Overmeere, T. Pardoen, *Acta Mater.* **2017**, *125*, 27.
[7] Covestro AG, Makrolon®ISO Datasheet, Makrolon® 2408, https://solutions.covestro.com/en/products/makrolon/makrolon-2408_00013320-05123200?SelectedCountry=DE, (accessed: April **2024**).
[8] V. D. Jadhav, A. J. Patil, B. Kandasubramanian, in *Handbook of Consumer Nanoproducts*, (Eds.: S. Mallakpour, C. M. Hussain), Springer Nature, Singapore **2022**, 257.
[9] S. Shi, S. Qian, X. Hou, J. Mu, J. He, X. Chou, *Adv. Condens. Matter Phys.* **2018**, *2018*, 7598978.
[10] H.-J. Liu, C.-H. Huang, C.-Y. Chen, S.-W. Hsiao, Y.-S. Chen, M.-H. Lee, Y.-C. Chen, P.-J. Wu, M.-W. Chu, J. G. Lin, *Phys. Status Solidi Rapid Res. Lett.* **2020**, *14*, 2000273.
[11] S. Seo, S. Shin, E. Kim, S. Jeong, N.-G. Park, H. Shin, *ACS Energy Lett.* **2021**, *6*, 3332.
[12] E. J. Frankberg, J. Kalikka, F. García Ferré, L. Joly-Pottuz, T. Salminen, J. Hintikka, M. Hokka, S. Koneti, T. Douillard, B. Le Saint, P. Kreiml, M. J. Cordill, T. Epicier, D. Stauffer, M. Vanazzi, L. Roiban, J. Akola, F. Di Fonzo, E. Levänen, K. Masenelli-Varlot, *Science* **2019**, *366*, 864.
[13] S. Ebnesajjad, A. H. Landrock, in *Adhesives Technology Handbook*, Elsevier, Amsterdam, Netherlands **2015**, 1.
[14] G. Beamson, D. Briggs, *High resolution XPS of organic polymers: The Scienta ESCA300 database*, Wiley, Chichester **1992**.
[15] T. O. Kääriäinen, D. C. Cameron, M. Tanttari, *Plasma Process. Polym.* **2009**, *6*, 631.
[16] L. J. Gerenser, *J. Vac. Sci. Technol. A* **1988**, *6*, 2897.
[17] S. Ben Amor, G. Baud, M. Jacquet, G. Nansé, P. Fioux, M. Nardin, *Appl. Surf. Sci.* **2000**, *153*, 172.
[18] A. Moustaghfir, E. Tomasella, E. Bêche, J. Cellier, M. Jacquet, *Plasma Process. Polym.* **2007**, *4*, S359.
[19] M. Hans, PhD thesis, RWTH Aachen University, Aachen, Germany **2017**.
[20] D. Manova, J. W. Gerlach, S. Mändl, *Materials* **2010**, *3*, 4109.
[21] J. T. Gudmundsson, *Plasma Sources Sci. Technol.* **2020**, *29*, 113001.
[22] A. Anders, *J. Appl. Phys.* **2017**, *121*, 171101.
[23] Creative Commons, CC BY 4.0 DEED, Attribution 4.0 International, https://creativecommons.org/licenses/by/4.0/ (accessed: April 2024).
[24] L. Patterer, P. Ondračka, D. Bogdanovski, S. Mráz, S. Karimi Aghda, P. J. Pöllmann, Y.-P. Chien, J. M. Schneider, *Adv. Mater. Interfaces* **2023**, *10*, 2300215.
[25] K. Momma, F. Izumi, *J. Appl. Crystallogr.* **2011**, *44*, 1272.
[26] M. C. Burrell, J. J. Chera, *Surf. Sci. Spectra* **1999**, *6*, 1.
[27] L. Patterer, P. Ondračka, D. Bogdanovski, L. Jende, S. Prünte, S. Mráz, S. Karimi Aghda, B. Stelzer, M. Momma, J. M. Schneider, *Appl. Surf. Sci.* **2022**, *593*, 153363.
[28] L. Patterer, S. Kollmann, T. de los Arcos, L. Jende, S. Karimi Aghda, D. M. Holzapfel, S. A. Salman, S. Mráz, G. Grundmeier, J. M. Schneider, *J. Vac. Sci. Technol. A: Vac. Surf. Films* **2023**, *41*, 053112.
[29] B. Putz, T. E. Edwards, E. Huszar, P. A. Gruber, K.-P. Gradwohl, P. Kreiml, D. M. Többens, J. Michler, *Adv. Eng. Mater.* **2023**, *25*, 2200951.
[30] A. A. Taylor, M. J. Cordill, L. Bowles, J. Schalko, G. Dehm, *Thin Solid Films* **2013**, *531*, 354.
[31] G. Beamson, D. Briggs, *High resolution XPS of organic polymers, The Scienta ESCA300 database*, Wiley, Chichester **1992**.
[32] G. Greczynski, L. Hultman, *J. Appl. Phys.* **2022**, *132*, 11101.
[33] P. Stoyanov, S. Akhter, J. M. White, *Surf. Interface Anal.* **1990**, *15*, 509.
[34] A. L. Allred, *J. Inorg. Nucl. Chem.* **1961**, *17*, 215.
[35] B. Putz, G. Milassin, Y. Butenko, B. Völker, C. Gammer, C. Semprimoschnig, M. J. Cordill, *Surf. Coat. Technol.* **2017**, *332*, 368.
[36] J. E. Klemberg-Sapieha, D. Poitras, L. Martinu, N. L. S. Yamasaki, C. W. Lantman, *J. Vac. Sci. Technol. A: Vac. Surf. Films* **1997**, *15*, 985.
[37] D. A. Shirley, *Phys. Rev. B.* **1972**, *5*, 4709.
[38] XPS sensitivity factors for AXIS Supra, Kratos Analytical Ltd. (accessed: December 2023).
[39] T. Ozaki, *Phys. Rev. B.* **2003**, *67*, 155108.
[40] T. Ozaki, H. Kino, *Phys. Rev. B.* **2004**, *69*, 195113.
[41] T. Ozaki, H. Kino, *Phys. Rev. B.* **2005**, *72*, 045121.
[42] K. Lejaeghere, G. Bihlmayer, T. Björkman, P. Blaha, S. Blügel, V. Blum, D. Caliste, I. E. Castelli, S. J. Clark, A. Dal Corso, S. de Gironcoli, T. Deutsch, J. K. Dewhurst, I. Di Marco, C. Draxl, M. Dułak, O. Eriksson, J. A. Flores-Livas, K. F. Garrity, L. Genovese, P. Giannozzi, M. Giantomassi, S. Goedecker, X. Gonze, O. Grånäs, E. K. U. Gross, A. Gulans, F. Gygi, D. R. Hamann, P. J. Hasnip, et al., *Science* **2016**, *351*, aad3000.
[43] J. P. Perdew, K. Burke, M. Ernzerhof, *Phys. Rev. Lett.* **1996**, *77*, 3865.

[44] S. Grimme, J. Antony, S. Ehrlich, H. Krieg, *J. Chem. Phys.* **2010**, *132*, 154104.
[45] T. Ozaki, C.-C. Lee, *Phys. Rev. Lett.* **2017**, *118*, 26401.
[46] C. Draxl, M. Scheffler, *MRS Bull.* **2018**, *43*, 676.
[47] P. Ondračka, D. Bogdanovski, NOMAD dataset: Bond formation at polycarbonate | X interfaces (X = Al2O3, TiO2, TiAlO2) studied by theory and experiments - ab initio calculations, https://doi.org/10.17172/NOMAD/2023.03.31-1 (accessed: March **2023**).
[48] R. Dronskowski, P. E. Bloechl, *J. Phys. Chem.* **1993**, *97*, 8617.
[49] V. L. Deringer, A. L. Tchougréeff, R. Dronskowski, *J. Phys. Chem. A* **2011**, *115*, 5461.
[50] S. Maintz, V. L. Deringer, A. L. Tchougréeff, R. Dronskowski, *J. Comput. Chem.* **2013**, *34*, 2557.
[51] R. Nelson, C. Ertural, J. George, V. L. Deringer, G. Hautier, R. Dronskowski, *J. Comput. Chem.* **2020**, *41*, 1931.
[52] G. Kresse, J. Hafner, *Phys. Rev. B.* **1993**, *47*, 558.
[53] G. Kresse, J. Hafner, *Phys. Rev. B.* **1994**, *49*, 14251.
[54] G. Kresse, J. Furthmüller, *Phys. Rev. B.* **1996**, *54*, 11169.
[55] G. A. Landrum, R. Dronskowski, *Angew. Chem., Int. Ed.* **2000**, *39*, 1560.
[56] S. Steinberg, R. Dronskowski, *Crystals* **2018**, *8*, 225.